Applied Physics B (2026) 132:55
https://doi.org/10.1007/s00340-026-08665-6

Applied Physics B
Lasers and Optics

RESEARCH

Graphene based mesa metamaterials for detection of terahertz waves

Yasemin Demirhan[1,2] · Sinan Eroglu[1] · Necip Ayhan Tertemiz[3] · Sinan Balci[3] · Hakan Altan[4] · Lutfi Ozyuzer[1,5]

Received: 3 November 2025 / Accepted: 23 March 2026
© The Author(s) 2026

Abstract

A high performance terahertz (THz) metamaterial structure based on graphene is presented, exploiting hybrid dielectric graphene resonances to achieve tunable resonance frequencies. Graphene coated mesa metamaterial structures were designed and fabricated on a single chip, enabling strong electromagnetic field confinement and tunable response without the need for additional metamaterial layers. The proposed architecture provides a compact and efficient platform for tunable THz photodetection and opens new possibilities for next generation graphene based plasmonic devices. The metamaterial unit cells were optimized using CST Microwave Studio simulations to operate at target frequencies of 1.1, 0.9, and 0.8 THz, respectively. Device fabrication was performed on high resistivity silicon substrates via UV lithography and reactive ion beam etching, followed by graphene deposition using chemical vapor deposition (CVD). The electromagnetic responses of the fabricated devices were characterized using a continuous-wave THz imaging system. The effects of graphene thickness and Fermi level on the reflection spectra were investigated, and the hybrid dielectric graphene resonance modes were qualitatively analysed and compared with the experimental results. By integrating graphene conformally onto three dimensional dielectric mesa resonators, enhanced light–matter interaction and tunable hybrid resonances can be achieved. The proposed plasmonic enhanced metamaterial detector provides a promising platform for future bio-THz sensing applications.

1 Introduction

The terahertz (THz) region of the electromagnetic spectrum remains a relatively underexplored domain, yet it offers immense potential for both electronic and photonic applications. Generally defined as the frequency range between 0.1 and 10 THz ($\lambda \approx 3$–30 μm) [1], this spectral window has enabled significant innovations in medical imaging [2], wireless communication [3–5], security screening [6, 7], military surveillance [8, 9], and landmine detection [10]. Over the past two decades, advances in materials science have facilitated the development of efficient THz sources and detectors, further underscoring the importance of this frequency range. Notable technological breakthroughs include strong THz signal generation via time-domain spectroscopy (TDS), THz imaging systems, and nonlinear optical effects [11]. Consequently, research efforts have increasingly focused on two main objectives: (1) achieving high-power THz radiation and (2) realizing fast, sensitive THz detection. Our previous work has contributed to the advancement of high power THz generation techniques [12], while other major milestones have been reported in both passive and active THz devices [13–18]. With the growing demand for powerful sources and recognition of THz technology's potential in advanced physical research and commercial applications, far infrared and THz systems have undergone transformative progress. More recently, THz and infrared technologies have expanded into emerging fields such as nanomaterials science, biochemistry, and post-5G communications, driven by the fact that THz frequencies coincide with the energy scales of both individual and collective excitations in nanoelectronics and biomolecular systems. Although compact,

✉ Yasemin Demirhan
yasemindemirhan@iyte.edu.tr

1 Department of Physics, Izmir Institute of Technology, 35430 Urla, Izmir, Turkey

2 Center for Materials Research, Integrated Research Centers, Izmir Institute of Technology, 35430 Urla, Izmir, Turkey

3 Department of Photonics, Izmir Institute of Technology, 35430 Urla, Izmir, Turkey

4 Department of Physics, Middle East Technical University, 06800 Ankara, Turkey

5 Teknoma Technological Materials Inc., Teknopark Izmir, 35430 Urla, Izmir, Turkey

Published online: 04 April 2026

solid-state devices for THz wave generation, manipulation, and detection have been realized, they still face challenges in integration, sensitivity, and cost-effectiveness, hindering widespread adoption in THz photonics. The THz band also exhibits several distinctive properties: THz radiation can penetrate many non-metallic, dielectric materials without ionization, making it highly suitable for non-invasive medical diagnostics and security imaging. For instance, THz imaging can detect concealed weapons beneath clothing or identify early-stage skin abnormalities through molecular spectral signatures. Moreover, extending Wi-Fi and wireless communication frequencies into the sub THz regime (above 100 GHz) could greatly increase data bandwidth; however, this advancement depends on the development of highly sensitive, low noise THz detectors and scalable, cost-efficient fabrication methods. At the core of terahertz (THz) photodetection and other optoelectronic technologies lies the fundamental principle of converting incident photons into electrical signals. Consequently, THz photodetectors are indispensable in applications such as medical imaging, security screening, quality control, and molecular spectroscopy [19, 20]. One of the principal advantages of THz radiation is its non-ionizing nature: it operates at photon energies in the millielectronvolt (meV) range, unlike X-rays, which lie in the kiloelectronvolt (keV) regime and pose health risks through ionization.

Terahertz (THz) photonics has become a rapidly expanding field bridging quantum optics, materials science, and bio photonics. THz radiation, located between the microwave and infrared regions of the electromagnetic spectrum, interacts sensitively with low energy molecular vibrations, hydrogen bonding, and water absorption in biological tissues.

These unique properties make THz waves highly attractive for label-free, non-invasive imaging and spectroscopy of biomolecules, cells, and soft tissues. Consequently, the development of efficient, tunable, and miniaturized THz detectors is essential for advancing next generation bio photonic sensing platforms. In this context, metamaterial based and plasmonic enhanced detector architectures offer new opportunities to achieve strong field confinement, frequency selectivity, and high detection sensitivity, which are crucial for bio-THz applications.

Beyond imaging and sensing, THz detectors are expected to play a pivotal role in the development of next-generation THz band wireless communication systems. An ideal THz detector should fulfil five essential performance criteria: (i) high sensitivity (i.e., low noise-equivalent power, NEP), (ii) room temperature operation, (iii) fast photo response, (iv) wide dynamic range (from the weakest to the strongest detectable signals) and (v) broadband spectral responsivity across the THz band. In this context, two dimensional (2D) materials have emerged as promising candidates for next-generation THz photodetectors. Among them, graphene has attracted particular attention due to its exceptional electronic and optoelectronic properties. Its linear energy momentum dispersion enables ultrafast charge transport with a Fermi velocity approximately 1/100 that of light. Furthermore, graphene exhibits remarkably high carrier mobility (up to 20,000 $cm^2\ V^{-1}\ s^{-1}$ at room temperature) making it ideally suited for high-speed THz detection. Its atomically thin structure also confers an ultra-low volume and heat capacity, beneficial for achieving single-photon sensitivity and ultrafast response times.

To exploit these exceptional characteristics in practical devices, graphene must be integrated with suitable supporting architectures. In this regard, metamaterial structures, engineered to manipulate electromagnetic waves in ways unattainable by natural materials, have garnered significant attention [21–25]. Dielectric based metamaterials are advantageous in the THz regime owing to their low intrinsic losses, enabling precise tuning of electromagnetic responses and enhanced light matter interactions.

Recent advances in graphene integrated metamaterials have revealed their immense potential for terahertz (THz) photodetection, owing to their ability to support highly tunable plasmonic resonances and strong electromagnetic field confinement. By coupling the exceptional carrier dynamics of graphene with the engineered resonance properties of metamaterials, it becomes possible to realize photodetectors with enhanced responsivity and spectral selectivity [26–28].

The integration of graphene layers with metallic or dielectric frequency selective metasurfaces was initially explored in the mid infrared regime [29]. When graphene is positioned atop a metamaterial architecture, a pronounced shift in the transmission dependent spectral response emerges as a consequence of the strong electromagnetic coupling between the conductive graphene layer and the underlying passive photonic resonators. In the terahertz (THz) frequency domain, hybrid metamaterial graphene platforms have been proposed for the realization of ultra sensitive detectors, wherein dynamic tunability is achieved through modulation of graphene's Fermi energy [30]. Subsequent theoretical investigations have introduced tunable dielectric metamaterial resonator configurations patterned directly on graphene surfaces for THz operation. These resonators exhibit polarization insensitive behavior and wide angle robustness, enabling both broadband and dual band absorption characteristics. Such properties render the proposed architectures particularly suitable for advanced applications, including high-resolution sensing, THz imaging, and active modulation [31].

In 2018, a pioneering theoretical study demonstrated that graphene itself can be engineered into a metamaterial

platform capable of ultra-sensitive detection through the excitation of multiple plasmonic resonance modes [32]. In this approach, compact three dimensional dielectric prism like structures were conformally coated with graphene, thereby forming a three dimensional graphene-based metamaterial operating within the 2–6 THz frequency range. Numerical simulations revealed the emergence of three distinct absorption resonances with absorption efficiencies exceeding 95%. The principal novelty of this work lies in transforming three dimensional dielectric architectures into functional metamaterials via graphene coating, as opposed to integrating graphene onto prefabricated planar metamaterial surfaces. Moreover, active tuning of the graphene Fermi level enabled precise control over the resonance frequencies, with the corresponding resonance sensitivity surpassing that of previously reported metamaterial-based sensing platforms.

Experimentally, various graphene/metamaterial hybrid architectures have been reported, including metallic split-ring resonators and periodic dielectric arrays, which significantly improve light matter interactions in the THz domain [33–36]. Nevertheless, most of these designs rely on planar or multilayer configurations where graphene is transferred onto pre-patterned metamaterial surfaces, often leading to fabrication challenges, poor adhesion, and reduced coupling efficiency. To overcome these limitations, experimental efforts are increasingly focused on developing more robust and scalable integration techniques that can enhance the electromagnetic interaction while maintaining device simplicity and reproducibility.

The incorporation of metamaterial resonators significantly enhances local electromagnetic field confinement and resonance quality, thereby amplifying light matter interaction within the graphene layer. Strong plasmonic coupling in hybrid metamaterial systems leads to elevated carrier densities in the absorption region, resulting in markedly improved responsivity and detection sensitivity. Furthermore, the spectral tunability of hybrid plasmonic modes enables spectrometer-free detection schemes, while the monolithic integration of metamaterials facilitates the development of compact, low cost, and high performance sensor platforms.

Despite the demonstrated advantages of graphene plasmonic metamaterial hybrids in achieving fast response times, high sensitivity, and scalable fabrication, two critical challenges remain unresolved: the reliable integration of graphene with subwavelength metamaterial elements and the precise, active control of graphene's electronic and optical properties to modulate the overall electromagnetic response of hybrid plasmonic devices. Addressing these challenges necessitates a paradigm shift toward alternative detector architectures, rather than conventional hybrid designs in which metamaterial structures are integrated as post fabrication components.

This study presents graphene integrated dielectric metamaterials specifically designed for THz photodetection applications. In contrast to conventional planar or multilayer graphene metamaterial systems, this work focuses on the integration of monolayer graphene with three-dimensional dielectric mesa structures.

The novelty of the approach lies in the mesa type geometry and its interaction with graphene, rather than in the graphene transfer process itself. This approach enhances the interaction between THz waves and graphene, while preserving device simplicity and integrity. It should be emphasized that the graphene transfer process itself follows well established procedures; the primary contribution of this work is the demonstration of optically tunable terahertz response enabled by the three-dimensional mesa dielectric metamaterial architecture. The proposed structure is not intended to support isolated graphene plasmon polaritons, which typically require nanoscale graphene patterning. Instead, the novelty lies in the three dimensional integration of a continuous graphene layer with dielectric silicon mesa resonators, forming a hybrid graphene dielectric metasurface in the sub THz/THz regime. The silicon mesas support Mie type and cavity modes, while graphene acts as a tunable conductive surface that modulates the resonance strength and damping via its frequency dependent surface conductivity. The observed resonances are therefore hybrid dielectric graphene modes dominated by silicon mesa cavities rather than pure graphene plasmons. The results demonstrate that the proposed device structure exhibits strong absorption, minimal reflection, and broadband operation across the THz spectrum.

2 Experimental

2.1 Design and fabrication of mesa materials

2.1.1 Numerical design and CST simulation of graphene integrated THz metamaterials

The design and optimization of terahertz (THz) mesa structures were conducted using CST Microwave Studio, a comprehensive electromagnetic simulation platform capable of modelling wave matter interactions in both time and frequency domains. CST provides critical insights into resonance behaviour, absorption efficiency, and overall device performance, making it particularly suitable for metamaterial based THz applications. The simulation model utilized materials selected from CST's built in library and defined within the software environment. The mesa-type

metamaterial structure consists of patterned graphene, patterned silicon mesas, a silicon substrate, and a gold back reflector. The structure was analysed using the frequency-domain solver under unit cell boundary conditions, allowing accurate characterization of the periodic response. During numerical analyses, S_{11} (reflection) parameters were extracted to evaluate resonance performance. Mesa dimensions were optimized for target resonance frequencies of 0.8, 0.9, and 1.2 THz, corresponding to lateral dimensions of 115 μm × 115–135 μm × 135 μm, 86 μm × 86–101 μm × 101 μm, and 70 μm × 70–90 μm × 90 μm, respectively. Prior to fabrication, detailed simulations were conducted to study the effects of mesa height, unit cell spacing, and layer thickness on resonance performance.

For the periodic metasurface structures, the unit cell geometry was defined using two parameters: the mesa size **a** and the lattice periodicity **b**, as illustrated schematically in Fig. 1. For the target resonance frequencies of 1.2, 0.9, and 0.8 THz, the mesa dimensions **a** were set to 70 μm, 86 μm, and 115 μm, respectively. The corresponding unit-cell periodicities **b** were chosen as 90 μm, 101 μm, and 135 μm. Accordingly, the unit-cell sizes were $70 \times 90\ \mu m^2$ (1.2 THz), $86 \times 101\ \mu m^2$ (0.9 THz), and $115 \times 135\ \mu m^2$ (0.8 THz). The metasurfaces were fabricated on a silicon substrate with a thickness ($\mathbf{t_s}$) of 200 μm, relative permittivity $\varepsilon_r = 3$, relative permeability $\mu_r = 1$, and loss tangent $\tan\delta = 0.01$. The mesa height is denoted as $\mathbf{t_m}$, as shown in Fig. 1. A 200 nm thick gold film was deposited on the backside of the substrate to serve as a reflective layer.

In the simulation setup, periodic boundary conditions were applied along the x- and y-axes to represent an infinite periodic array of unit cells, while open (add space) boundaries were used along the z-axis to allow free space propagation of THz waves. A normally incident plane wave was employed as the excitation source, with the electric field polarized along the x-direction and the magnetic field along the y-direction, ensuring that the induced surface currents and plasmonic resonances were effectively coupled to the graphene layer.

The frequency domain solver was selected for its ability to accurately capture steady-state electromagnetic behaviour across the THz spectrum. The simulation frequency range was set between 0.4 and 1.5 THz, encompassing the designed resonance frequencies. A fine adaptive mesh was used around the graphene and silicon interface to ensure convergence and precise calculation of localized field enhancements. From the simulated reflection parameter (S_{11}), the absorption (A) spectrum was calculated using the relation

$$A(\omega) = 1 - |S_{11}|^2,$$

assuming negligible transmission due to the gold back reflector. The resulting absorption peaks correspond to the resonant modes of the graphene integrated dielectric metamaterial structure.

The graphene layer was modelled using the Drude conductivity model, which effectively captures the intraband carrier dynamics in the THz regime. The surface conductivity of graphene, σ(ω), was defined as

$$\sigma(\omega) = \left(e^2 E_F\right) / \left(\pi\hbar^2\right) \times 1/(\tau - i\omega)$$

where E_F is the Fermi level, τ is the carrier relaxation time, e is the elementary charge, $\hbar$ is the reduced Planck constant, and ω is the angular frequency. The Fermi level was set to 0.6 eV, and the carrier relaxation time to 0.5 ps, consistent with room temperature measurements for

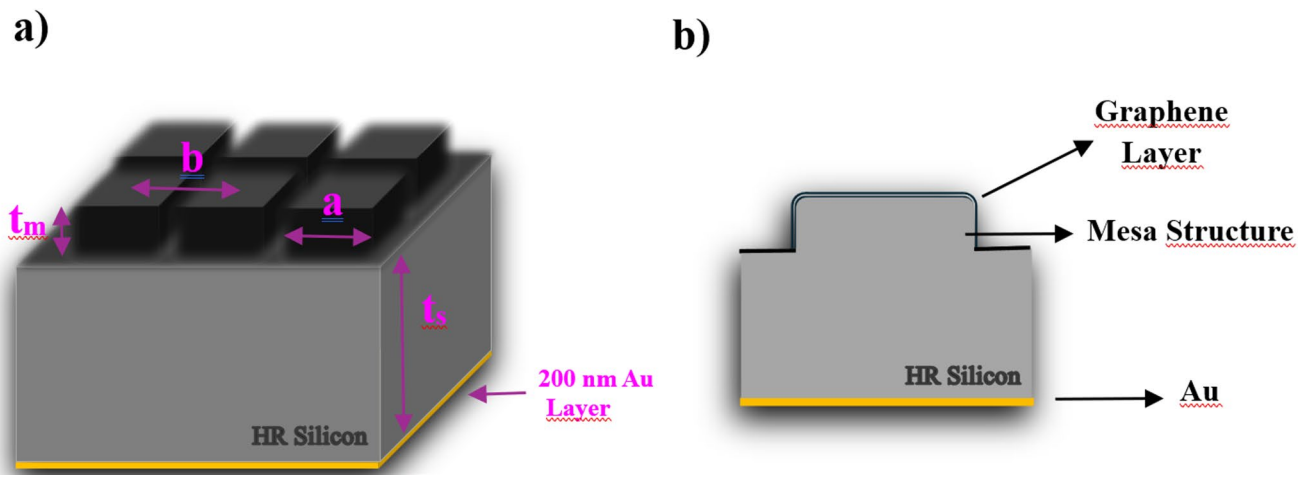


Fig. 1 **a** Three-dimensional schematic illustration of the proposed metasurface unit cell, showing the lateral mesa dimension **a**, unit cell periodicity **b**, mesa height $\mathbf{t_m}$, and substrate thickness $\mathbf{t_s}$. **b** Cross sectional side view of the unit cell illustrating the layered structure consisting of the graphene layer, silicon mesa structure fabricated on a high resistivity (HR) silicon substrate, and a 200 nm thick Au reflector

CVD-grown graphene. The graphene layer was treated as 1 nm thick to maintain accurate electromagnetic coupling while minimizing computational load. Following the simulation stage, the optimized designs were experimentally fabricated and characterized to validate the predicted optical response and tunability, demonstrating their suitability as optically tunable THz metasurfaces with potential applications in photodetection.

2.2 Fabrication process of mesa metamaterials

The fabrication of the mesa structures was carried out using the geometrical parameters determined through simulations. The mesa metamaterial structures were successfully fabricated on the surface of high resistivity (HR) silicon wafers for the corresponding frequencies using photolithography and ion beam etching techniques. The microstructural features and resonance frequencies of the surfaces were realized in accordance with the optimum unit cell parameters and mesa heights determined from the numerical analyses.

A negative photoresist (AZ5214E) was spin coated onto the thin film substrates at 3000 rpm to achieve uniform thickness. The coated substrates were subsequently soft baked on a hotplate at 110 °C for 90s to remove residual solvents. The desired chiral patterns were defined by exposing the photoresist coated substrates to ultraviolet (UV) light for 20s through a pre-designed photomask. A developer solution consisting of 100 mL of deionized water and 0.8 g of NaOH was prepared to selectively dissolve the UV exposed regions of the photoresist. The samples were immersed in the developer for 20s to remove the developed areas, followed by rinsing with deionized water and drying under a nitrogen stream. The unexposed photoresist regions, protected by the photomask, were then hard baked at 110 °C for 30 min to ensure complete curing and adhesion. Prior to pattern transfer, the ion beam etching (IBE) chamber was evacuated to a base pressure of 3.0×10^{-6} Torr using a two-stage pumping system consisting of a roughing pump and a turbomolecular pump (TMP). During the etching process, argon gas was introduced at a controlled flow rate of 30 sccm to generate a stable plasma for anisotropic material removal.

Following the lithography and etching processes, graphene was transferred onto the patterned mesa structures to enable tunable plasmonic functionality. Monolayer graphene synthesized via chemical vapor deposition (CVD) on a copper foil was utilized as the active material. The transfer process employed a polymethyl methacrylate (PMMA)-assisted wet transfer method. A thin PMMA layer was first spin-coated onto the graphene/copper substrate and subsequently baked at 100 °C for 2 min to enhance adhesion. The underlying copper foil was then etched using an aqueous ammonium persulfate (APS) solution (0.1 M) until complete removal of the metal layer was achieved. The PMMA/graphene film was carefully rinsed several times with deionized water to eliminate residual etchants and subsequently transferred onto the target patterned substrate.

After the transfer process, the sample was dried at room temperature for 12 h to promote conformal contact between the graphene and the underlying microstructure surface. The PMMA support layer was then dissolved by immersing the sample in an acetone bath for 1 h, followed by rinsing with isopropyl alcohol (IPA) and drying under a nitrogen stream. Raman spectroscopy and optical microscopy were employed to confirm the integrity and uniformity of the transferred graphene layer. Finally, a thin gold (Au) film with a thickness of 200 nm was deposited on the backside of the substrate by thermal evaporation to provide optical reflectivity enhancement. The complete structure was then annealed at 200 °C for 30 min under a nitrogen atmosphere to improve the interfacial adhesion and electrical conductivity between layers.

The fabricated metamaterial samples were characterized to verify their structural integrity, surface morphology, and optical performance. The surface topology and microstructural features of the patterned mesa structures were examined using field-emission scanning electron microscopy (FE-SEM, JEOL JSM-7001 F). Raman spectroscopy (Renishaw in Via, 532 nm excitation) was performed to confirm the monolayer nature and crystalline quality of the graphene film, with the G and 2D band intensities analysed to assess layer uniformity and defect density. The optical and electromagnetic responses of the metasurfaces were investigated using a CW terahertz system operating in the 0.3–0.8 THz range. The experimental results were compared with the numerical simulations obtained from the frequency-domain solver in CST Studio Suite to validate the design accuracy.

Figure 2 presents the SEM images of the fabricated mesa type metamaterial structures at different magnifications. The overall morphology demonstrates a highly uniform and periodic array of square shaped resonators successfully formed after the fabrication process. At low magnification, the large area uniformity and well defined periodic pattern indicate the effectiveness of the lithography and etching parameters in transferring the designed structure onto the substrate. Higher magnification images reveal that the mesas possess sharp and smooth edges without noticeable deformation or surface defects, confirming the high accuracy of the fabrication process. The lateral dimensions of the square features are approximately 68–70 μm, which closely match the design values.

This dimensional accuracy ensures consistent electromagnetic behaviour across the structure and is crucial for achieving the intended resonance characteristics of the

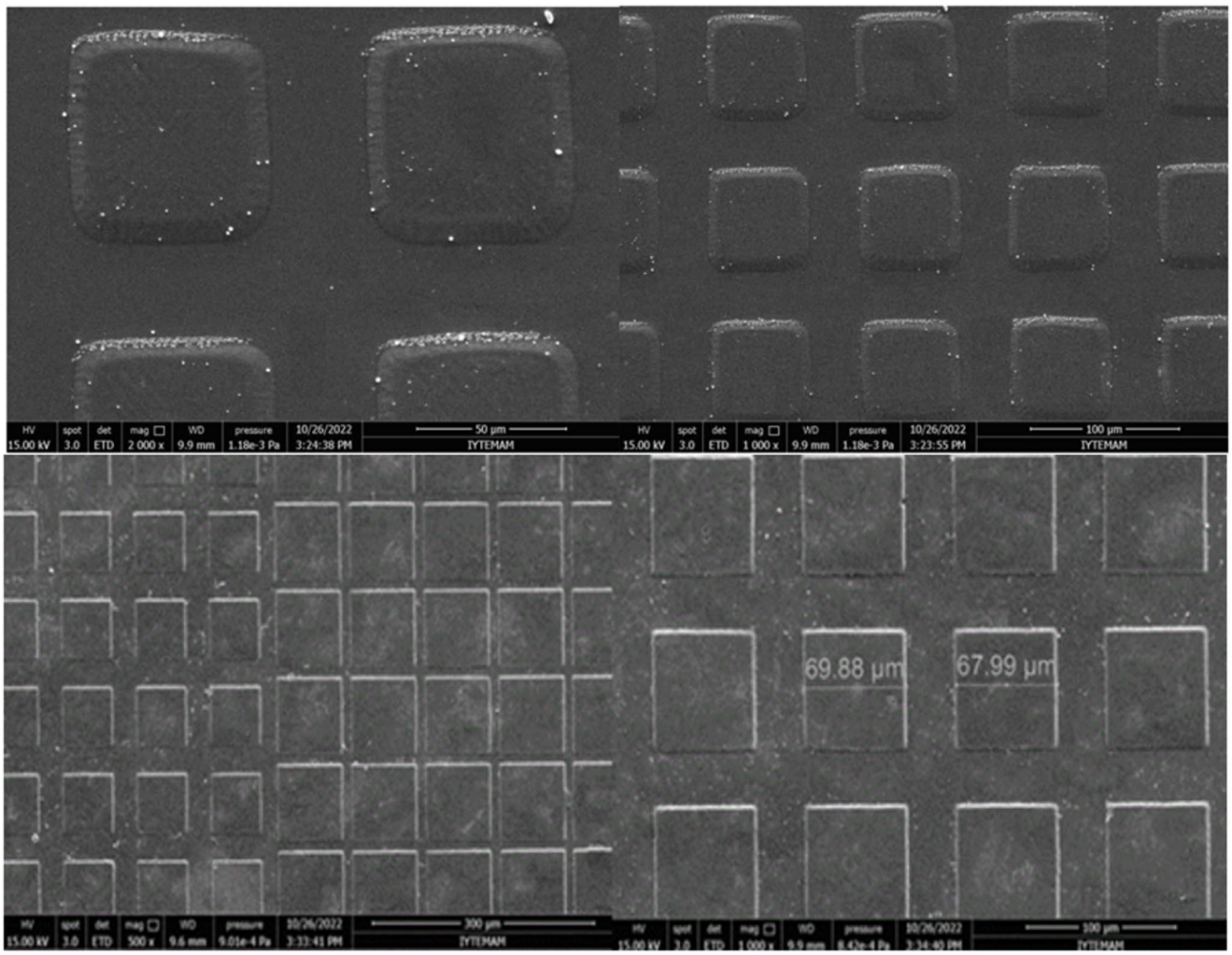


Fig. 2 SEM images of the mesa metamaterial structures taken at different magnifications after the fabrication process

metamaterial array. The clean and uniform morphology also indicates good adhesion between layers and minimal process induced damage, demonstrating the reliability of the employed fabrication method (Fig. 3).

The Raman mapping scan was performed using a Renishaw Raman microscope with a 532 nm excitation laser under ambient conditions. The line-scan map (10 µm in length) shows consistent graphene Raman features along the scanned region, indicating good spatial uniformity of the film. The dominant 2D band with minimal variation across the scan further confirms the monolayer nature of the graphene.

2.3 Experimental setup for THz measurements

Figure 4 illustrates the schematic of the terahertz (THz) measurement setup [24]. The characterization of the fabricated mesa metamaterials was performed using a continuous-wave terahertz (CW-THz) system at İzmir Institute of Technology (İYTE). The experimental setup integrates a frequency-tunable THz source, an RF function generator, a frequency counter, and a VDI WR1.5 AMC (Virginia Diodes, Inc. WR1.5 Amplified Multiplier Chain), capable of generating THz radiation in the 0.500–0.750 THz frequency range. Sample positioning is facilitated by a precision x-y translation stage driven by stepper motors, controlled via Leadshine drivers and MC USB201 controller. The stage movement is automated through a LabVIEW interface, enabling accurate scanning along both axes. THz waves emitted from the WR1.5 AMC source are modulated at 15 Hz with a 2.5 V peak-to-peak TTL signal generated by a Stanford Research Systems DS335 function generator.

The beam is focused using a Teflon lens with a 10 cm focal length to optimize the incident power on the metasurface samples. To reduce undesired emissions, the source is equipped with a cross-horn antenna ensuring directional radiation. Samples measuring 8×8 mm^2 were mounted

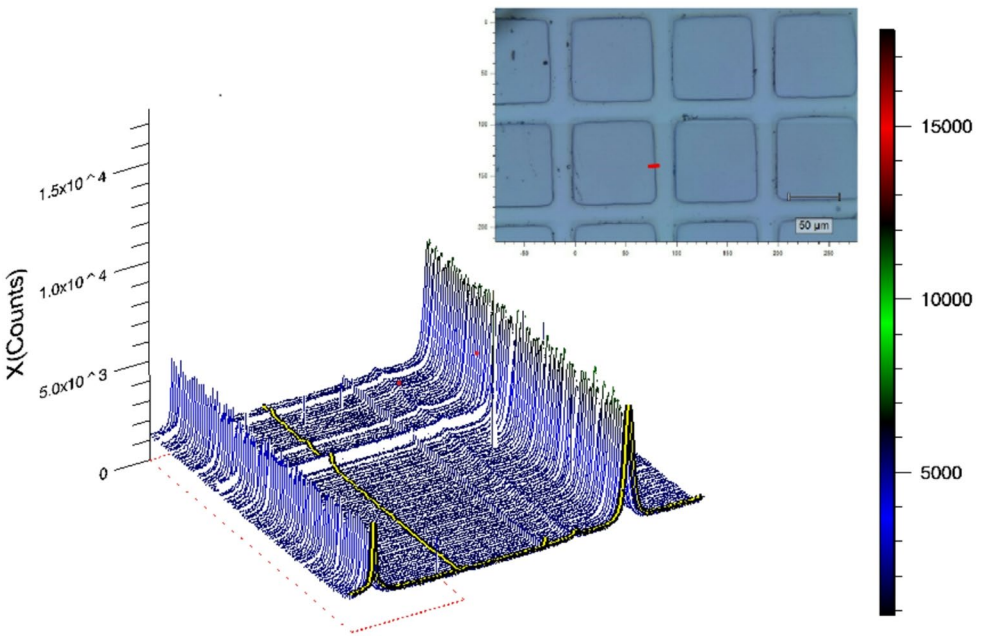


Fig. 3 Three dimensional Raman line scan mapping of monolayer graphene acquired along the dashed red line shown in the inset optical image

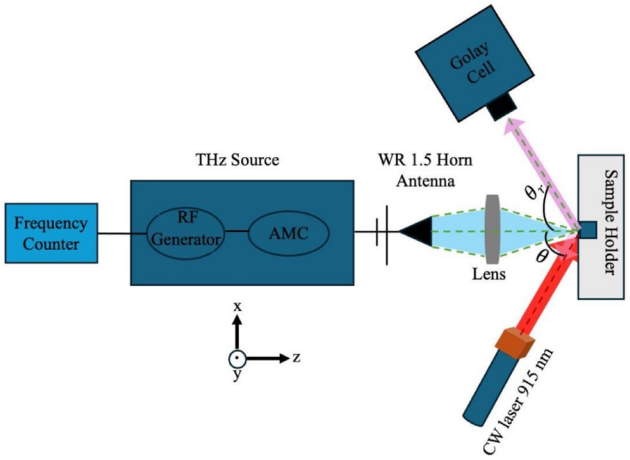


Fig. 4 Schematic view of the experimental setup [24]

on the translation stage to allow normal incidence of the beam onto the metasurface. The reflected THz signal was collected by a Golay cell detector, with signal amplification and lock-in detection carried out using a Stanford Research Systems 830 lock-in amplifier. The beam diameter was set to approximately 44 mm, providing sufficient coverage of the sample surface. Optical alignment was critically performed using 90° off-axis parabolic mirrors, ensuring minimal signal loss by maintaining precise mechanical and focal alignment between the THz source, scanning stage, and Golay detector. Initial x-y scans were conducted to confirm sample positioning before spectral measurements. Spectral data were collected by sweeping the THz frequency from 500 GHz to 750 GHz in 1 GHz increments. Baseline measurements were performed to characterize the ambient air spectrum, followed by systematic measurements of the metasurface samples to evaluate their THz response. This setup provides high sensitivity and spatial resolution for detailed characterization of THz metamaterials, enabling comprehensive analysis of their frequency dependent electromagnetic properties.

3 Results and discussion

3.1 Design and simulation of mesa metamaterials

Simulated reflection spectra of the metamaterial absorber for different mesa thicknesses (values indicated in the legend) is given in Fig. 5. It is clearly seen that the thickness controls the resonant impedance and loss balance, leading to systematic shifts in the reflection minimum and changes in absorption bandwidth. The results indicate that while the resonance frequency remains nearly constant around 0.9 THz, the resonance intensity exhibits a clear dependence on the pillar thickness. The strongest resonance is obtained for $t = 6.96$ µm, suggesting optimal coupling between the graphene layer and the underlying Si mesa. Both thinner and thicker structures exhibit reduced resonance depth, which can be attributed to impedance mismatch and weaker plasmonic confinement.

These results confirm that fine tuning the mesa thickness is essential for achieving strong and high quality resonant behaviours in the designed metasurface structure. While the resonance frequency remains nearly fixed, increasing mesa thickness systematically broadens the low reflection bandwidth and deepens the minimum. This is attributed to enhanced modal overlap and increased dissipative loss in

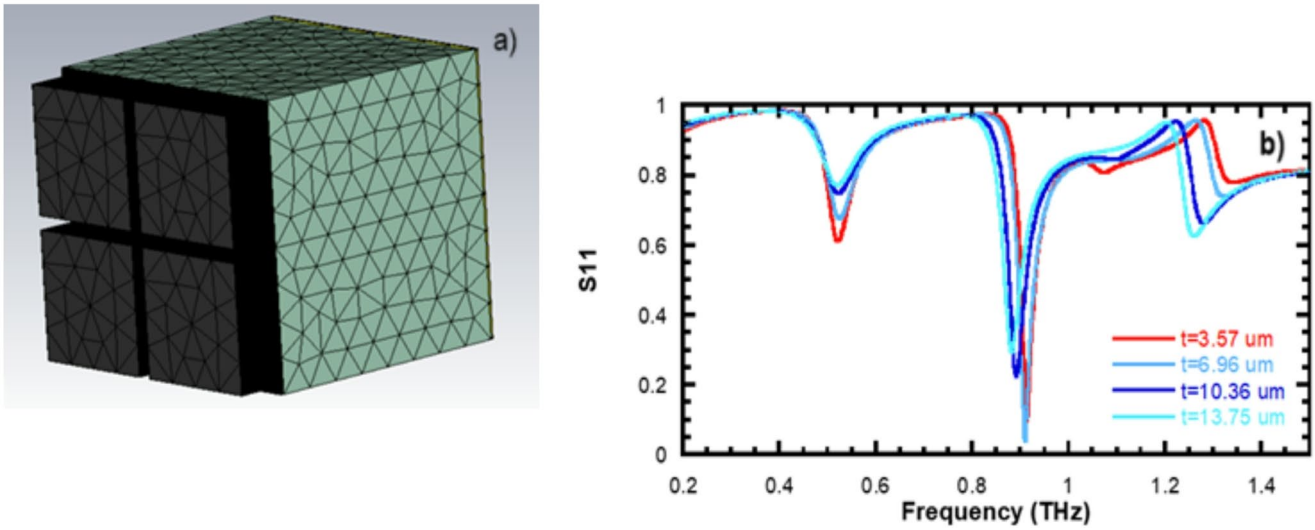


Fig. 5 **a** CST simulation model of the unit cell structure consisting of a graphene layer, 86 × 86 µm mesa pillar, 101 × 101 µm mesa pillar, and a gold layer, shown for different mesa pillar thicknesses (t = 3.57 µm, 6.96 µm, 10.36 µm, and 13.75 µm) as designed in the program interface, **b** S11 simulation results of the unit cell structure composed of a graphene layer, 86 × 86 µm mesa pillar, 101 × 101 µm mesa pillar, and a gold layer, obtained for different mesa pillar thicknesses (t = 3.57 µm, 6.96 µm, 10.36 µm, and 13.75 µm)

the resonator, which flattens the reflection dispersion around resonance. The resulting absorber is less sensitive to fabrication tolerances and frequency drift.

These trends are consistent with the LC resonant nature of the metasurface and cavity effects between the patterned layer and ground plane: modifying mesa thickness tunes the effective inductance/capacitance and the optical path, thereby controlling impedance matching to free space and the loss balance that handle absorption.

Figure 6a, b illustrates the effect of graphene's Fermi energy and Si mesa geometry on the reflection characteristics (S_{11}) of the proposed unit cell. Variation of the graphene Fermi energy primarily modulates the resonance strength and damping, whereas the resonance frequency remains nearly unchanged due to the dominant role of the dielectric mesa geometry. This behaviour originates from the modulation of graphene's surface conductivity, which directly influences the plasmonic resonance within the hybrid metasurface. The graph further reveals that varying the mesa thickness also affects the resonance strength and position, indicating that both geometrical and electrical parameters can be used to dynamically control the terahertz response. These results demonstrate the potential of combining tunable materials and geometrically engineered designs to achieve broadband and reconfigurable polarization control in the terahertz regime.

Figure 6c and d show the simulated electric field distributions at the resonance frequencies for different mesa dimensions. In both cases, the electric field is strongly localized within the silicon mesa cavities and is particularly enhanced near the mesa edges and graphene–semiconductor interfaces. The back gold layer acts as a reflector, reinforcing field confinement inside the mesa without directly contributing to plasmonic excitation.

A comparison between the two geometries indicates that smaller mesa dimensions lead to higher peak electric field intensities, consistent with stronger electromagnetic confinement. These observations confirm that the dominant resonance is a dielectric cavity (Mie-type) mode modulated by the presence of graphene, rather than a pure graphene plasmon. Figure 6 provides the numerical basis for interpreting the experimental results shown in Figs. 7, 8, 9 and 10. The simulations demonstrate how variations in graphene conductivity and silicon mesa geometry affect the resonance depth and spectral response of the metasurface. The experimental spectra in Figs. 7, 8, 9 and 10 correspond to fabricated samples with mesa dimensions consistent with the simulated designs. Although graphene modulation is achieved experimentally via laser induced photothermal effects rather than electrostatic gating, the resulting changes in resonance strength and damping follow the same conductivity dependent trends predicted by the simulations.

The absolute resonance frequencies obtained from simulations are expected to differ from the experimental values due to simplified material models and idealized excitation conditions; however, the simulations reliably capture the underlying mode structure and tuning trends.

Figure 7 presents the THz reflection spectra of the unpatterned and mesa metamaterial samples in the 500–750 GHz range. In Figs. 7, 8, 9 and 10, the reflected signals are presented as normalized reflection intensity rather than absolute reflectance, as obtained from the CW THz measurement

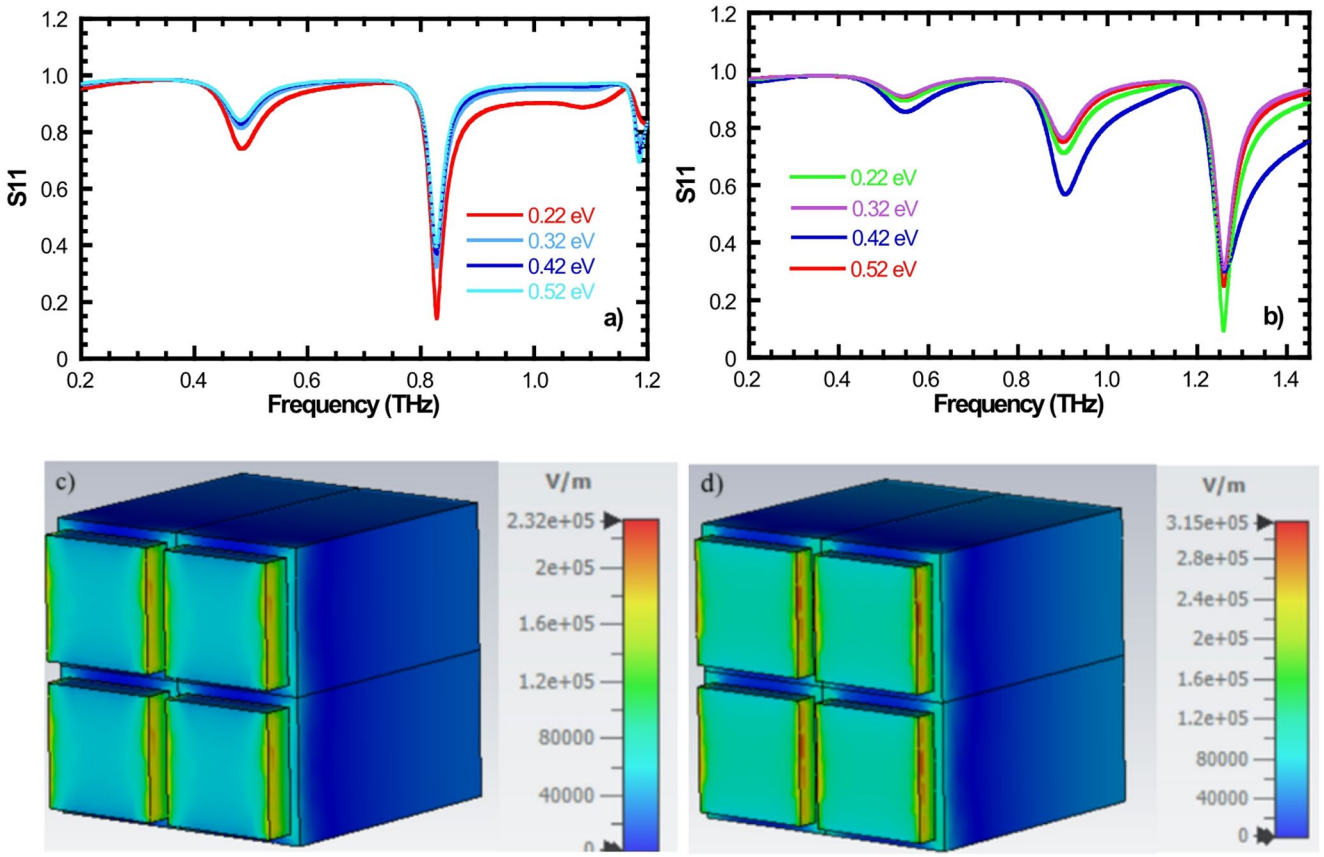


Fig. 6 **a** S11 simulation results of the unit cell structure composed of a graphene layer, 115 × 115 μm mesa, 135 × 135 μm mesa, and a gold layer, obtained for different Fermi energy levels of graphene at a fixed mesa thickness (t = 22.81 μm). **b** S11 simulation results of the unit cell structure composed of a graphene layer, 70 × 70 μm mesa, 90 × 90 μm mesa, and a gold layer, obtained for different Fermi energy levels of graphene at a fixed mesa thickness (t = 17.42 μm). **c** and **d** show the simulated electric field distributions at the resonance frequencies

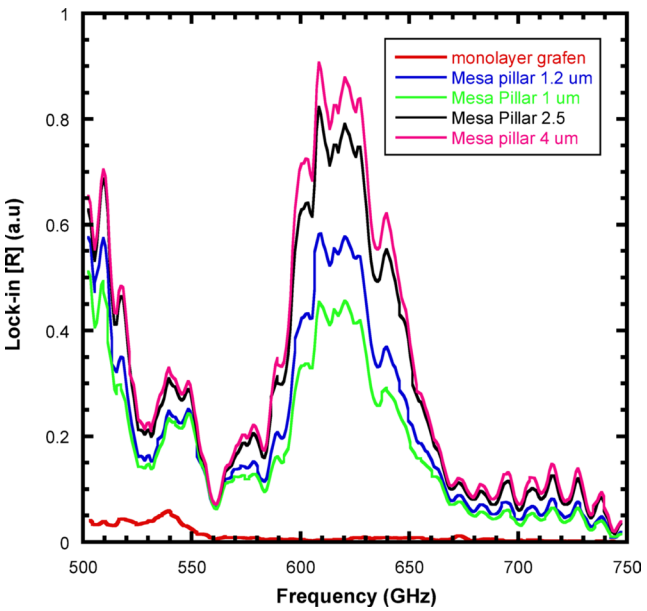


Fig. 7 The THz reflection spectra of the unpatterned graphene/Si/Au reference sample and the samples with different mesa heights, measured in the frequency range of 500–750 GHz, are presented on the same graph

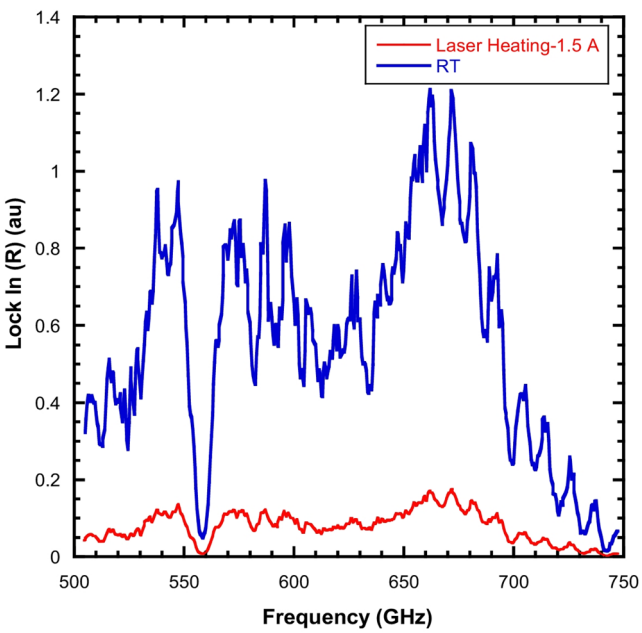


Fig. 8 THz reflection spectrum measured between 500 and 750 GHz for a mesa pillar structure (85 μm × 85 μm) integrated with monolayer graphene

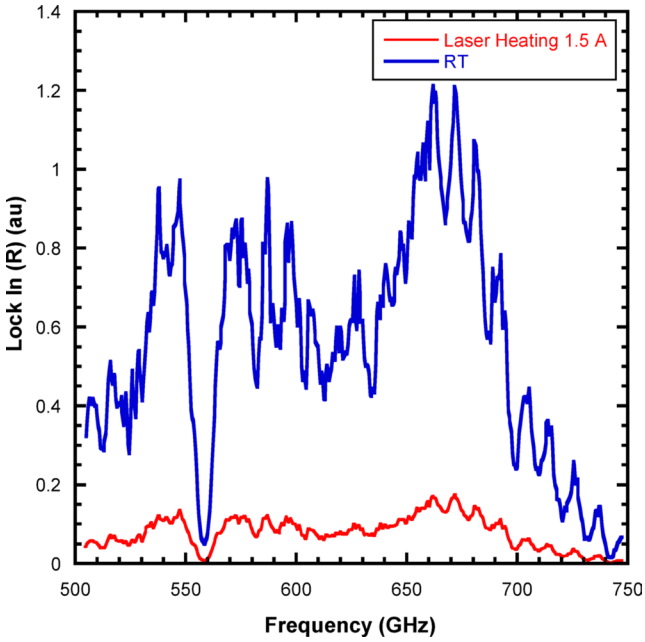


Fig. 9 THz reflection spectrum measured between 500 and 750 GHz for a mesa pillar structure (115 µm × 115 µm) integrated with monolayer graphene, obtained at room temperature and under laser illumination (plotted on the same graph)

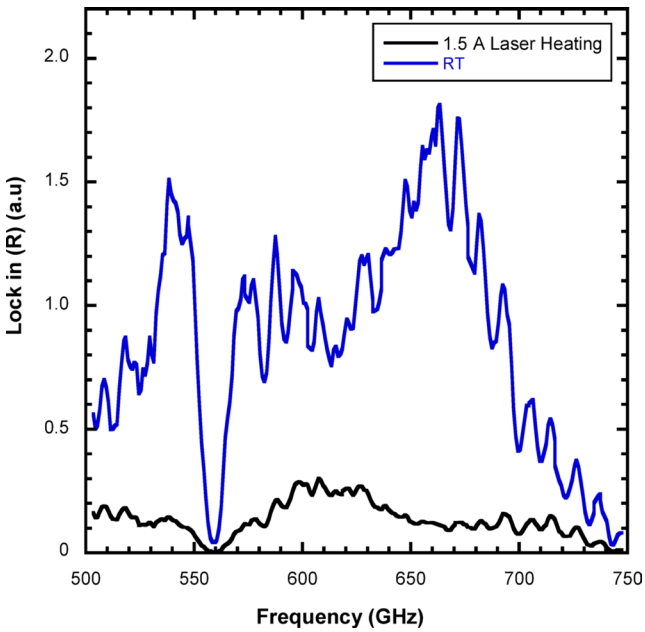


Fig. 10 THz reflection spectrum measured between 500 and 750 GHz for a mesa pillar structure (70 µm × 70 µm) integrated with monolayer graphene, obtained at room temperature and under laser illumination (plotted on the same graph)

system. The mesa metamaterial samples exhibit distinct reflection dips compared to the unpatterned surface, indicating resonance formation. A redshift in the resonance frequency with increasing mesa height suggests enhanced field confinement and an extended optical path within the structure. The reference monolayer graphene exhibits negligible reflection across the spectrum, confirming its strong absorption capability. In contrast, introducing silicon mesa pillars significantly modifies the resonance behaviour. As the mesa height increases from 1.0 to 4.0 µm, the reflection magnitude increases and pronounced resonance peaks emerge, particularly around 600–640 GHz. This trend indicates that thicker mesas enhance cavity effects and modify the effective optical path length, leading to stronger impedance mismatch with free space. While lower mesa heights (1.0–1.2 µm) provide relatively broadband, moderate reflection, higher pillars (2.5–4.0 µm) introduce sharp resonant features with higher reflection amplitude, which can be attributed to increased modal confinement and stronger Fabry Pérot like resonances within the pillar-substrate cavity.

These observations confirm that pillar thickness is a key parameter for tailoring the reflective and absorptive properties of the structure for THz applications.

Figure 8 presents the reflection spectrum of a monolayer graphene sheet transferred onto a mesa metamaterial structure under laser excitation. The structure was illuminated with a continuous-wave laser at a wavelength of 915 nm and a power of 50 mW. Under 50 mW continuous wave laser illumination, graphene experiences a moderate photothermal temperature rise (on the order of several tens of kelvin), which primarily modifies its complex surface conductivity through enhanced carrier–phonon scattering and thermal carrier redistribution. Such conductivity modulation is sufficient to induce the observed changes in resonance depth and reflection amplitude, without requiring a large shift in the graphene Fermi level.

The observed spectral modulation under laser illumination originates from photothermal effects in graphene, which modify its surface conductivity rather than providing direct electrostatic control of the Fermi level [37–39]. Compared to the unexcited state, a small but detectable redshift of the resonance minimum is observed in the 0.6–0.75 THz frequency range. This spectral modulation is attributed primarily to optically induced photothermal effects in graphene, which modify the carrier temperature and scattering rate, leading to changes in its complex surface conductivity.

The resulting conductivity modulation alters the plasmonic resonance conditions of the hybrid graphene–mesa metamaterial, giving rise to tunable reflection behaviour. In addition to the frequency shift, an increase in the resonance depth and reflection contrast is observed under laser illumination, indicating enhanced light matter interaction between the graphene layer and the underlying mesa metasurface. These results demonstrate that optical excitation provides an effective and reversible approach for dynamic tuning of terahertz reflection properties in graphene-based

metasurfaces, highlighting their potential for reconfigurable terahertz devices and active photonic components. The observed spectral modulation under laser illumination is consistent with previously reported behavior in graphene based hybrid metasurfaces, where optically induced conductivity enhancement leads to a small redshift of the resonance frequency and concurrent changes in resonance strength [40].

Figure 9 presents the reflection spectrum of the laser excited mesa metamaterial structure integrated with monolayer graphene. Experimental results revealed that graphene-based mesa metamaterial structures exhibit tunable optoelectronic properties when illuminated by a laser beam [37]. The measurement results demonstrate that graphene coated metamaterial structures are promising candidates for dynamically controllable THz devices operating at room temperature [38, 39]. In addition, a reduction in the scattering mechanism was observed under laser illumination, which was attributed to the change in the plasmonic behaviour of the graphene layer upon optical excitation [40]. The higher experimental reflection values compared to numerical simulations can mainly be attributed to the ideal plane wave model used in the simulations, which does not fully represent the focused beam conditions of the experimental setup, as well as to micron scale alignment errors that may occur during the microfabrication process. These discrepancies should be considered as important parameters when comparing simulation and experimental results.

Measurements performed on the mesa structure with dimensions of 70 μm × 70 μm revealed distinct resonance peaks in the frequency range of 500–750 GHz (Fig. 10). The reflection spectra obtained at room temperature indicate that the monolayer graphene exhibits strong electromagnetic interaction despite its single-atomic thickness. After laser illumination, a slight frequency shift of the resonance peak and an increase in reflection amplitude were observed. This behaviour is attributed to the thermally induced excitation caused by laser illumination, which increases the carrier concentration in the graphene layer and shifts its Fermi level upward. The measured spectrum confirms that the mesa geometry at this scale effectively supports plasmonic resonances.

The THz reflection characteristics of the fabricated mesa metamaterial structures were systematically investigated as a function of mesa height and lateral dimensions. As shown in Figs. 7, 8, 9 and 10, the introduction of silicon mesa pillars strongly modifies the spectral response compared to the unpatterned substrate, leading to the appearance of distinct resonance features within the 500–750 GHz frequency range.

Increasing the mesa height results in a redshift of the resonance frequency and an increase in reflection amplitude, which can be attributed to enhanced field confinement and extended optical path length within the mesa–substrate cavity. Integration of monolayer graphene onto the mesa metamaterial surface further enhances the light matter interaction. Despite its atomic thickness, graphene exhibits strong coupling with the localized THz fields, resulting in tunable reflection spectra. Under laser illumination (915 nm, 50 mW), the reflection resonances exhibit a noticeable redshift and amplitude enhancement, originating from photocarrier generation and thermally induced modulation of the Fermi level in graphene. These effects demonstrate the dynamic control of the plasmonic response through optical excitation, confirming that the hybrid mesa structures act as optically reconfigurable THz elements.

In addition to the localized resonances supported by the silicon mesa structures, the experimental spectra in Figs. 7, 8, 9 and 10 exhibit weak oscillatory features that can be attributed to Fabry–Pérot type interference within the silicon substrate and the mesa substrate cavity. These oscillations arise from multiple internal reflections between the mesa layer and the gold back reflector and are enhanced by the high refractive index and finite thickness of the silicon substrate. The combination of geometrical tunability and optically induced modulation highlights the potential of these structures for THz bio photonic applications. Since THz radiation is highly sensitive to molecular vibrations, hydration levels, and biological tissue composition, the demonstrated platform can serve as a basis for label free sensing and real time bio-diagnostic systems. The strong field localization within the mesa cavities and the optical tunability provided by graphene make this architecture a promising candidate for next generation active, reconfigurable THz bio photonic devices. The terahertz reflection characteristics of the fabricated mesa metamaterial structures were systematically investigated as a function of mesa height, lateral dimensions, and graphene integration. As shown in Figs. 7, 8, 9 and 10, the introduction of silicon mesa pillars significantly modifies the spectral response compared to the unpatterned graphene reference, leading to the emergence of distinct resonance features within the 500–750 GHz frequency range. Increasing the mesa height results in a gradual redshift of the resonance frequency and an enhancement of the reflection amplitude, which can be attributed to stronger electromagnetic field confinement and an extended effective optical path length within the mesa substrate cavity. Variations in the lateral dimensions further influence the resonance sharpness and spectral position by modifying the modal distribution and cavity conditions. The integration of monolayer graphene onto the mesa metamaterial surface enhances the light matter interaction despite its atomic thickness. Under optical excitation (915 nm, 50 mW), all graphene-integrated structures exhibit consistent

and reversible modulation of the reflection spectra, characterized by a small but detectable redshift of the resonance minimum and an increase in resonance depth.

This behavior originates primarily from optically induced photothermal effects in graphene, which modify its complex surface conductivity and alter the plasmonic resonance conditions of the hybrid structure. In addition to the localized resonances supported by the mesa pillars, weak oscillatory features observed in the experimental spectra can be attributed to Fabry–Pérot type interference within the silicon substrate and the mesa substrate cavity, arising from multiple internal reflections between the mesa layer and the gold back reflector. Overall, the combined effects of geometrical tunability and optical modulation demonstrate that the proposed graphene integrated mesa metamaterials function as optically reconfigurable terahertz elements, offering promising potential for active THz devices, sensing platforms, and future biophotonic applications.

4 Conclusion

In summary, graphene coated dielectric metamaterial mesa pillars have been successfully designed and fabricated to achieve tunable, high performance terahertz (THz) photodetection. By directly integrating graphene onto mesa type dielectric features, the proposed architecture enables efficient plasmonic coupling and enhanced light matter interaction without the need for additional metamaterial layers. This approach not only simplifies the fabrication process but also improves the optical absorption and responsivity across a broad THz frequency range. The demonstrated structure exhibits enhanced absorption behaviour, low reflection, and strong field confinement, highlighting its potential for room temperature, high sensitivity, and fast response THz detection. Moreover, the inherent tunability of graphene's Fermi level allows dynamic control over the resonance characteristics, offering a versatile platform for adaptive THz devices. The metamaterial unit cells were optimized using simulations to operate at target frequencies of 1.2, 0.9, and 0.8 THz, with dimensions of (70×70 μm^2–90×90 μm^2), (85×85 μm^2–100×100 μm^2), and (115×115 μm^2–135×135 μm^2), respectively.

Mesa type metamaterial structures were designed to function as active resonant elements, enabling the development of an optically tunable THz metasurface architecture that extends beyond conventional metamaterial detector integration and provides a platform for future photodetection implementations. The electromagnetic responses of the fabricated devices were measured using continuous wave terahertz systems. These results pave the way for the development of next-generation, chip integrated, graphene based plasmonic systems suitable for advanced applications in spectroscopy, communication, imaging, and sensing. Owing to its sensitivity to optical stimuli and strong field localization, the proposed structure can be potentially extended to label free biological sensing, molecular fingerprinting, and real time diagnostic systems operating in the THz regime. Future work will focus on optimizing the mesa geometry and graphene doping level to further enhance modulation depth and response speed, enabling integration into compact THz devices.

Acknowledgements This research is partially supported by TUBITAK (Scientific and Technical Research Council of Turkey) project number 221M087. We would like to thank the Research and Application Center for Quantum Technologies (RACQUT) of IZTECH.

Author contributions Y.D.: Conceptualization, Methodology, Fabrication, Writing—Original draft preparation, S.E.: Fabrication N.A.T.: Fabrication, L.Ö, H.A, S.B: Conceptualization, Visualization, L.Ö: Supervision, Reviewing and Editing.

Data availability Data is provided within the manuscript.

Declarations

Conflict of interest The authors declare no conflict of interest.

Open Access This article is licensed under a Creative Commons Attribution-NonCommercial-NoDerivatives 4.0 International License, which permits any non-commercial use, sharing, distribution and reproduction in any medium or format, as long as you give appropriate credit to the original author(s) and the source, provide a link to the Creative Commons licence, and indicate if you modified the licensed material. You do not have permission under this licence to share adapted material derived from this article or parts of it. The images or other third party material in this article are included in the article's Creative Commons licence, unless indicated otherwise in a credit line to the material. If material is not included in the article's Creative Commons licence and your intended use is not permitted by statutory regulation or exceeds the permitted use, you will need to obtain permission directly from the copyright holder. To view a copy of this licence, visit http://creativecommons.org/licenses/by-nc-nd/4.0/.

References

1. M. Tonouchi, Nat. Photon. **1**, 97 (2007)
2. D.M. Mittleman, M. Gupta, R. Neelamani et al., Appl. Phys. B **68**, 1085 (1999)
3. Z. Chen, C. Han, Y. Wu et al., IEEE Commun. Mag. **59**, 66 (2021)
4. Y. Huang, Y. Shen, J. Wang, Engineering. **22**, 106 (2023)
5. J. Federici, L. Moeller, J. Appl. Phys. **107**, 113102 (2010)
6. G. Tzydynzhapov, P. Gusikhin, V. Muravev et al., J. Infrared Millim. Terahertz Waves. **41**, 632 (2020)
7. A.V. Shchepetilnikov, P.A. Gusikhin, V.M. Muravev et al., J. Infrared Millim. Terahertz Waves. **41**, 655 (2020)
8. F.F. Sizov, Semicond. Phys. Quantum Electron. Optoelectron. **22**, 67 (2019)
9. M. Strąg, W. Świderski, Compos. Struct. **306**, 116 (2023)

10. A. Luukanen, E.N. Grossman, A.J. Miller et al., IEEE Microw. Wirel. Compon. Lett. **16**, 464 (2006)
11. V.E. Rogalin, I.A. Kaplunov, G.I. Kropotov, Opt. Spectrosc. **125**, 1053 (2018)
12. L. Ozyuzer, A.E. Koshelev, C. Kurter et al., Science. **318**, 1291 (2007)
13. K. Kadowaki, H. Yamaguchi, K. Kawamata et al., Phys. C **468**, 634 (2008)
14. S.K. Mathanker, P.R. Weckler, N. Wang, Trans. ASABE. **56**, 1213 (2013)
15. H.B. Wang, S. Guénon, B. Gross et al., Phys. Rev. Lett. **105**, 057002 (2010)
16. Y. Demirhan, H. Saglam, F. Turkoglu et al., Vacuum. **120**, 89 (2015)
17. Y. Demirhan, H. Alaboz, L. Ozyuzer, M.A. Nebioğlu, T. Takan, H. Altan, C. Sabah, Opt. Quantum Electron. **48**, 170 (2016)
18. Y. Demirhan, H. Alaboz, M.A. Nebioglu et al., Supercond Sci. Technol. **30**, 074006 (2017)
19. J.B. Baxter, G.W. Guglietta, Anal. Chem. **83**, 4342 (2011)
20. P.A. Banks, E.M. Kleist, M.T. Ruggiero, Nat. Rev. Chem. **7**, 480 (2023)
21. M.A. Nebioğlu, T. Takan, H. Altan et al., Mod. Phys. Lett. B **31**, 1750074 (2017)
22. S. Zeybek, Y. Demirhan, A. Noori et al., Mod. Phys. Lett. B **38**, 2450056 (2024)
23. B. Akyurek, A. Noori, Y. Demirhan et al., J. Infrared Millim. Waves. **46**, 5 (2025)
24. A. Noori, B. Akyurek, Y. Demirhan, L. Ozyuzer, K. Guven, H. Altan, G. Aygun, Opt. Quantum Electron. **55**, 676 (2023)
25. X. Li, X. Bian, W.I. Milne, D. Chu, Appl. Phys. B **122**, 95 (2016)
26. T. Semerci, Y. Demirhan, N. Miyakawa et al., NATO Sci. Peace Secur. Ser. B, 75 (2017)
27. B. Mulla, C. Sabah, Plasmonics. **11**, 1313 (2016)
28. A.S. Saadeldin, M.F.O. Hameed, E.M. Elkaramany et al., IEEE Sens. J. **19**, 7993 (2019)
29. B. Zeng, Z. Huang, A. Singh, Y. Yin, H. Arik, J. Dixon, X. Zhang, Light Sci. Appl. **7**, 51 (2018)
30. X. He, C. Sun, Y. Wang, G. Lu, J. Jiang, Y. Yang, Y. Gao, Nanomaterials. **11**, 2420 (2021)
31. H.-F. Huang, J.-Y. Wang, Crystals. **14**, 713 (2024)
32. X. Chen, W. Fan, C. Song, Carbon. **133**, 416–422 (2018)
33. S. Asgari, T. Fabritius, Sci. Rep. **14**, 7477 (2024)
34. M. Esfandiari, X. Lv, S. Chamani, Y. Yang, Mater. Today Electron. **11**, 100140 (2025)
35. P. Nasiri Shehni, M. Mehranpour, Appl. Opt. **64**, 2002–2008 (2025)
36. M. Esfandiari, J. Zhu, Y. Yang, APL Photon. **10**, 041101 (2025)
37. S. Krylow, F. Valencia Hernandez, B. Bauerhenne, M.E. Garcia, Phys. Rev. B **101**, 205428 (2020)
38. C. Ferrante, A. Virga, L. Benfatto et al., Nat. Commun. **9**, 308 (2018)
39. N. Yoshikawa, T. Tamaya, K. Tanaka et al., Science. **356**, 736–738 (2017)
40. G. Li, G. Wang, Y. Zhang, J. Shen, Y. Zhang, Nanoscale Adv. **5**, 756–766 (2023)

Publisher's note Springer Nature remains neutral with regard to jurisdictional claims in published maps and institutional affiliations.